A Letters Journal Exploring the Frontiers of Physics

August 2013

EPL, **103** (2013) 47006
doi: 10.1209/0295-5075/103/47006

www.epljournal.org

Electronic transport and photovoltaic properties in $Bi_2Sr_2Co_2O_y$ epitaxial heterostructures

Hai-Zhong Guo[1], Lin Gu[1], Zhen-Zhong Yang[1], Shu-Fang Wang[2(a)], Guang-Sheng Fu[2], Le Wang[1], Kui-Juan Jin[1(b)], Hui-Bin Lu[1], Can Wang[1], Chen Ge[1], Meng He[1] and Guo-Zhen Yang[1]

[1] *Beijing National Laboratory for Condensed Matter Physics, Institute of Physics, Chinese Academy of Sciences Beijing 100190, PRC*
[2] *College of Physics Science and Technology, Hebei University - Baoding 071002, PRC*

received 19 June 2013; accepted in final form 21 August 2013
published online 13 September 2013

PACS 73.40.Lq – Other semiconductor-to-semiconductor contacts, *p*-*n* junctions, and heterojunctions
PACS 73.40.-c – Electronic transport in interface structures
PACS 72.40.+w – Photoconduction and photovoltaic effects

Abstract – Epitaxial heterostructures constructed from the thermoelectric cobalt $Bi_2Sr_2Co_2O_y$ thin films and $SrTiO_3$ as well as $SrTi_{0.993}Nb_{0.007}O_3$ substrates were fabricated by pulsed-laser deposition. The scanning transmission electron microscopy results confirm that the heterostructures are epitaxial, with sharp and coherent interfaces. The temperature-dependent electrical transport properties and the Hall effects were systematically investigated. The $Bi_2Sr_2Co_2O_y/SrTi_{0.993}Nb_{0.007}O_3$ *p*-*n* heterostructure exhibits good rectifying current-voltage characteristics over a wide temperature range. A strong photovoltaic effect was observed in the $Bi_2Sr_2Co_2O_y/SrTi_{0.993}Nb_{0.007}O_3$ heterostructure, with the temperature-dependent photovoltage being systematically investigated. The present work shows a great potential of this new heterostructures as photoelectric devices.

In recent years, tremendous activities have been engaged to study the heterostructures of transition metal oxides, particularly for oxide electrical applications in which artificial multi-functionalities are used to realize novel devices [1,2]. Such oxide heterostructures possess an incredible variety of physical phenomena mainly due to the interface effects, such as unusual positive magnetoresistance [3,4], magnetocapacitance [5], photovoltage [6,7], electroresistance [8], interfacial superconductivity [9], two-dimensional electron gas [10], etc. The discovery of such remarkable electrical properties at the oxide interfaces has stimulated intensive research to explore new structures of the oxide heterostructures and utilize their novel electrical properties at the oxide interfaces.

Layered cobalt oxide $Bi_2Sr_2Co_2O_y$ (BSCO) exhibits a rather large thermoelectric power S ($\sim$130 μV/K) at room temperature, which makes BSCO be one of promising candidates for thermoelectric applications, analogous to other layered cobaltites such as Na_xCoO_2 and $Ca_3Co_4O_9$ [11–13]. Its crystal structure consists of alternating layers of the rock-salt $Bi_2Sr_2O_4$ subcell and the single CdI_2-type CoO_2 subcell stacked along the *c*-axis [11]. CdI_2-type CoO_2 subcells, in which electrons are strongly correlated, serve as electronic transport layers to achieve large thermoelectric power and low electrical resistivity, while the distorted rock-salt–type $Bi_2Sr_2O_4$ subcells enhance phonon scattering to achieve low thermal conductivity. For many microscale thermoelectric applications, thin films and heterostructures are highly desirable. Moreover, thin-film thermoelectric materials offer a tremendous scope for thermoelectric performance enhancement involving the use of quantum-confinement effects in quantum-dot structures, phonon-blocking/electron-transmitting in superlattices or thermionic effects in heterostructures [14]. In particular, thin films and heterostructures would provide the possibility of externally modifying the properties by epitaxial strain or artificial boundaries, and thus potentially generating novel properties at the interfaces, opening a new perspective for a variety of important experimental investigations [15]. In this work, BSCO heterostructures constructed from epitaxial $Bi_2Sr_2Co_2O_y$ thin films on

(a) E-mail: swang2008@hotmail.com
(b) E-mail: Kjjin@iphy.ac.cn

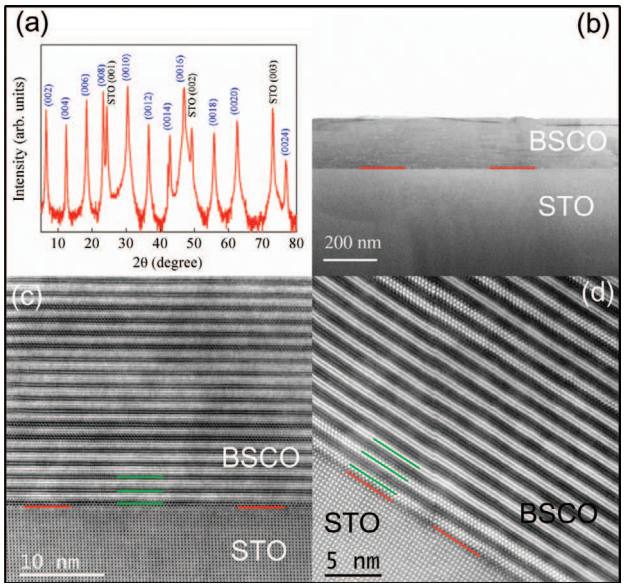

Fig. 1: (Color online) (a) XRD θ-2θ scan curves of the BSCO thin film on the STO substrate. (b) Low-magnification cross-section STEM images of BSCO film on the STO substrate. (c) A high-resolution ABF imaging and (d) a high-resolution HAADF imaging near the interface region showing the epitaxial growth of BSCO film on STO substrates. The interface is indicated by red lines, and the location of the CoO_2 layers is indicated by green lines.

$SrTiO_3$ (STO) and $SrTi_{0.993}Nb_{0.007}O_3$ (SNTO (0.7 wt%)) substrates were fabricated by pulsed-laser deposition (PLD), and the structural, electronic transport and photovoltaic properties of the heterostructures have been investigated.

Epitaxial 200-nm-thick BSCO films were grown on STO (001) and SNTO (0.7 wt%) (001) single-crystal substrates by the PLD technique [16,17]. The STO and SNTO substrates were carefully cleaned sequentially using alcohol, acetone, alcohol, and deionized water. Then, the substrates were dipped into an NH_4F buffered HF (4%) solution for 30 second so that the Sr-hydroxides are dissolved, leaving only TiO_2-terminated terraces [18]. The films were deposited at 680 °C using an excimer XeCl laser (1.5 J/cm^2, 308 nm, 3 Hz) at oxygen pressure of 40 mtorr. The crystalline quality of the BSCO thin films was analyzed using a X-ray diffraction (XRD) spectrometer with Cu Kα radiation. The XRD θ-2θ scan curve of the BSCO thin films is shown in fig. 1(a). Besides the peak from the STO (00l) substrate, only peaks from diffractions of the (00l) BSCO planes were observed, and no diffraction peaks from secondary phases or randomly oriented grains were detected, indicating that the thin films were grown along the c-axis with a good single phase.

To further characterize the crystalline structures of the BSCO heterostructures, state-of-the-art sophisticated aberration-corrected scanning transmission electron microscopy (STEM) techniques of the high-angle annular dark-field (HAADF) and annular bright-field (ABF) were utilized. Figure 1(b) shows the low-magnification cross-section STEM images of the BSCO thin film grown on the STO substrates. The BSCO film appears flat and homogeneous over large lateral distances. The epitaxial growth of the BSCO thin films on STO is confirmed by the high-resolution STEM images. Figures 1(c) and (d) show the ABF imaging and HAADF imaging near the interface region, respectively. It can be seen that the interface is sharp and coherent, without any evidence of secondary phases or chemical reaction in the interface region over large distances. This is against previous reports revealing that there always exist amorphous/delamination regions or buffer layers between BSCO or $Ca_3Co_4O_9$ films and substrates including $SrTiO_3$, $LaAlO_3$, Al_2O_3 and $(La_{0.3}Sr_{0.7})(AL_{0.65}Ta_{0.35})O_3$ (LAST) [19,20]. Sharp interface and no buffer layer at the interface of the BSCO heterostructures indicates the high quality of our BSCO heterostructures grown by PLD. Moreover, the alternating thick and thin clear contrast accounts for the SrO/BiO/BiO/SrO and CoO_2 layers, and the location of the CoO_2 layers is indicated by green lines in fig. 1(c). The c-axis orientation of the BSCO films can be confirmed with the SrO/BiO/BiO/SrO and CoO_2 layers parallel to the interface.

Resistivity and Hall effect measurements of the BSCO film were performed using a physical properties measurement system (PPMS, Quantum Design Inc.). The standard four-point probe method was used to measure in-plane resistivity (ρ) of the BSCO film grown on a STO substrate, and the resistivity results were shown in fig. 2(a). To make the ohmic contact, four platinum electrodes (0.5 mm in diameter) were deposited onto the films via thermal evaporation. The temperature dependence for the in-plane resistivity of the BSCO film exhibits a broad minimum around 140 K (seen in the inset of fig. 2(a)), exhibiting a broad transport crossover from the high-temperature metallic-like regime to the low-temperature insulating-like one. The diverging resistivity at low temperature has been attributed to the decrease of the density of states at Fermi level (E_F) due to a pseudogap formation below 30–50 K [21]. Hall effect measurement results were shown in fig. 2(b)–(d). The positive value of the Hall coefficient and positive slope of the Hall resistivity indicate the hole-like charge carriers of the BSCO. The Hall coefficient R_H exhibits a strong temperature dependence, as shown in fig. 2(b). The broad crossover of the temperature dependence of the Hall coefficient has also been observed at about 140 K, consistent with the results of the in-plane resistivity measurement. The Hall coefficient exhibits a sudden enhancement below low temperature, also suggesting a reduction of the density of states at Fermi level (E_F) due to a pseudogap formation at low temperature. This unconventional temperature dependence of the Hall coefficient for the BSCO film is believed to be related to the unusual electron correlations in BSCO. Note that similar results have also been observed in another layered cobalt

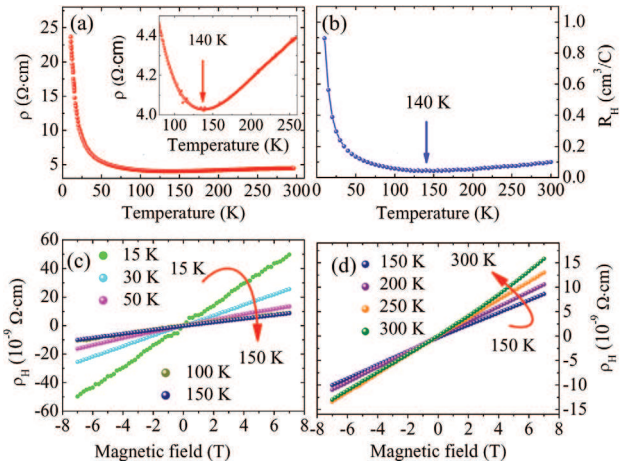

Fig. 2: (Color online) (a) Temperature dependence of the in-plane resistivity (ρ) of the BSCO film on the STO substrate. The inset shows a clear metal-insulator transition at $\sim 140\,\mathrm{K}$. (b) Temperature dependence of the Hall coefficient R_H of the BSCO film on the STO substrate under a magnetic field of $\pm 7\,\mathrm{T}$. Hall resistivity ρ_H *vs.* magnetic field below 150 K (c) and above 150 K (d).

oxide $Ca_3Co_4O_9$ [22]. Figures 2(c) and (d) show the Hall resistivity ρ_H *vs.* magnetic field below and above 150 K, respectively, around the metal-insulator transition temperature 140 K. The calculated hole carrier density of the BSCO film at room temperature is about $\sim 5\times10^{20}\,\mathrm{cm}^{-3}$.

The current-voltage (I-V) characteristics measurements on the BSCO/SNTO heterostructure were performed by two-probe technique to avoid the effects of current distribution in the junction (shown in the inset of fig. 3(a)). Ohmic contacts were prepared by evaporating gold electrodes with the diameter of $200\,\mu$m on the BSCO and SNTO, respectively. Figure 3(a) shows the typical current-voltage (I-V) characteristics of the BSCO/SNTO heterostructure at temperatures varying from 10 to 300 K. Good rectifying features characterized by asymmetric I-V curves are observed, which is similar to that of p-n diode made of a conventional semiconductor [23]. The temperature dependence of the diffusion voltage (V_D), defined by at that point the current starts to increase obviously, as a result of the application of a positive bias voltage, is shown in fig. 3(b). It can been seen from fig. 3(b) that V_D increases nearly linearly with decreasing temperature at high temperatures and then deviates from this behavior below 140 K, close to the metal-insulator transition temperature and the crossover temperature of the unusual temperature-dependent Hall coefficient of the BSCO layer. The deviation can be attributed to the decrease of the density of states at the Fermi level with decreasing temperature, and opening an energy gap across the Fermi level below the metal-insulator transition [24].

In fact, the BSCO layer exhibits a broad transport crossover from the high-temperature metallic-like regime to the low-temperature insulating-like one at around

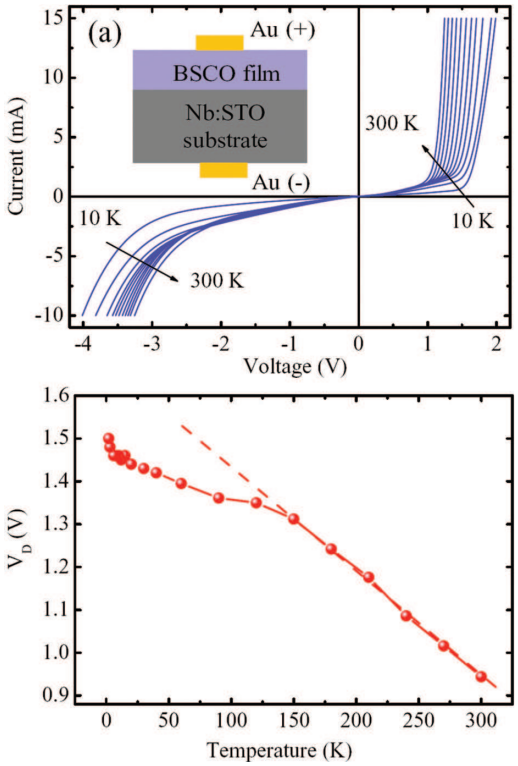

Fig. 3: (Color online) (a) Current-voltage characteristics of the BSCO/SNTO heterojunction in a temperature range from 10 K to 300 K with a temperature step of 30 K. The inset plot is the schematic diagram showing the electron setting. (b) Temperature-dependent diffusion voltage of the BSCO/SNTO heterostructures.

140 K, and Nb-doped $SrTiO_3$ (0.7 wt% doped) is an n-type degenerate semiconductor. Therefore, a Schottky heterojunction at high temperature and a (p-type)-BSCO-(n-type)-SNTO heterojunction at low temperature should be constructed when the BSCO layer is deposited onto the SNTO substrate. The electrons in n-type SNTO and holes in p-type BSCO layers should diffuse into the opposite regions due to the differences of carrier densities between n-type SNTO and p-type BSCO. The diffusion causes a built-in electric field in the space charge region around the interface, and a barrier at the interface. For simplicity of analysis, we assume hereafter that the BSCO/SNTO p-n heterojunction at low temperature can also be regarded as a Schottky heterojunction. This assumption is reasonable because we can take into account the fact that the carrier concentrations of the BSCO films ($\sim 5\times10^{20}\,\mathrm{cm}^{-3}$) and of the SNTO ($\sim 10^{19}\,\mathrm{cm}^{-3}$) at room temperature are generally large and the barrier width is correspondingly thin in transition-metal oxide heterojunctions comparing with the conventional semiconductor heterojunctions. The charge carriers can easily tunnel through the potential barrier to cross the junction instead of surmounting the potential barrier by thermal activating charge carriers.

Figure 4(a) displays a typical open-circuit transient photovoltage (PV) of the BSCO/SNTO heterostructure under

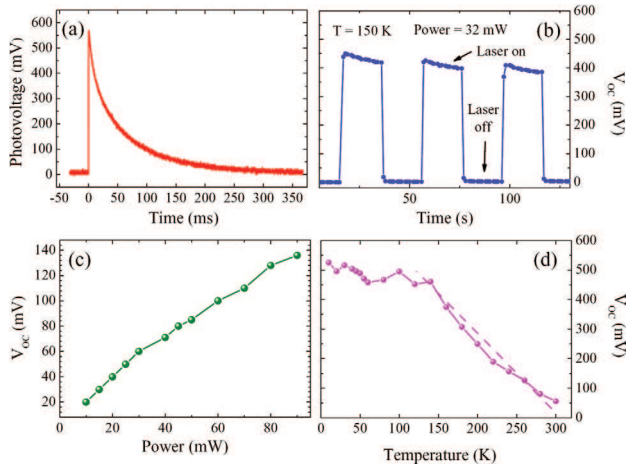

Fig. 4: (Color online) (a) Photovoltage of the BSCO/SNTO heterostructure with irradiation from the BSCO layer side by a 532 nm pulsed laser. (b) Steady photovoltage response of the BSCO/SNTO heterostructure under irradiation of a 532 nm cw laser at 150 K. (c) Photovoltage of the BSCO/SNTO heterostructure as a function of the power of a 532 nm cw laser. (d) Temperature-dependent photovoltages of the BSCO/SNTO under irradiation by 532 nm laser pulses. The dashed line is the guide for the eyes.

irradiation of a 532 nm pulsed laser at room temperature. The photoelectric signal was recorded by a 500 MHz digital oscilloscope with an input impedance of 1 MΩ. The BSCO crystal structure consists of alternating layers of the rock-salt SrO-BiO-BiO-SrO subcell $[(BiO)^{+}]$ and the single CdI_2-type CoO_2 $[(CoO_2)^{-}]$ subcell stacked along the *c*-axis; therefore BSCO is polar with alternately positively and negatively charged subcell layers along the *c*-axis. It has been recently proposed that an internal potential gradient exists in the polar $LaVO_3$ thin film in the $LaVO_3/SrTiO_3$ heterojunction, which can help to efficiently separate photoexcited electrons and holes as the photocarrier excitation takes places in the $LaVO_3$ region [25]. Under the scenario of the polar $LaVO_3/SrTiO_3$ heterojunction, with the illumination of light with the photon energy being larger than the band gap of BSCO, photon-induced carriers in the polar BSCO thin films are separated by a potential gradient inside BSCO regions, leading to a PV effect. Figure 4(b) shows the steady-state photoelectric response of the BSCO/SNTO heterostructure at the temperature of 150 K under the irradiation of a 532 nm continuous-wave (cw) laser. The photovoltage is high (low) when the laser is on (off). Figure 4(c) exhibits the relationship between the peak value of open-circuit photovoltage (V_{OC}) of the BSCO/SNTO heterostructure and the power density of the laser. The magnitude of V_{OC} increases linearly with the power density of the laser. The temperature-dependent V_{OC} of the BSCO/SNTO under the irradiation of a 532 nm cw laser is shown in fig. 4(d). It can been seen from fig. 4(d) that V_{OC} increases almost linearly with decreasing temperature from 300 to 140 K, and then deviates from this behavior below 140 K, almost consistent with the behavior of the temperature dependence of the diffusion voltage (V_D). This result is ascribed to the increase of the photo-induced carrier amount and the enhancement of the built-in electric field in the space charge region of the junction with the decrease of the temperature.

In summary, heterostructures constructed from the thermoelectric cobalt BSCO thin films and STO as well as SNTO substrates were fabricated by PLD. The epitaxial growth of the heterostructures is confirmed by high-resolution STEM images, exhibiting ultra-sharp and coherent interface. The results of the electrical transport and Hall effect measurements show that the BSCO layer exhibits a transport crossover from the high-temperature metallic-like regime to the low-temperature insulating-like behavior below 140 K. The BSCO/SNTO heterostructure exhibits good rectifying features over a large temperature range. Correspondingly, large photovoltages were observed under irradiation of a 532 nm laser, and the temperature dependence of the photovoltage was investigated. This work demonstrates that this thermoelectric heterostructures can be potentially applied in the optoelectronic devices.

* * *

This work was supported by the National Basic Research Program of China (Grant Nos. 2012CB921403 and 2013CB328706), the National Natural Science Foundation of China (Grant Nos. 10904030, 11004238, and 11134012), and Main Direction Program of Knowledge Innovation of Chinese Academy of Sciences (Grant No. YOV2021L31).

REFERENCES

[1] Heber J., *Nature*, **459** (2009) 28.
[2] Hwang H. Y., Iwasa Y., Kawasaki M., Keimer B., Nagaosa N. and Tokura Y., *Nat. Mater.*, **11** (2012) 103.
[3] Jin K. J., Lu H. B., Zhou Q. L., Zhao K., Cheng B. L., Chen Z. H., Zhou Y. L. and Yang G. Z., *Phys. Rev. B*, **71** (2005) 184428.
[4] Jin K. J., Lu H. B., Zhao K., Ge C., He M. and Yang G. Z., *Adv. Mater.*, **21** (2009) 4636.
[5] Nakagawa N., Asai M., Mukunoki Y., Susaki T. and Huang H. Y., *Appl. Phys. Lett.*, **86** (2005) 082504.
[6] Jin K. J., Zhao K., Lu H. B., Liao L. and Yang G. Z., *Appl. Phys. Lett.*, **91** (2007) 081906.
[7] Wang C., Jin K. J., Zhao R. Q., Lu H. B., Guo H. Z., Ge C., He M., Wang C. and Yang G. Z., *Appl. Phys. Lett.*, **98** (2011) 181101.
[8] Shang D. S., Sun J. R., Shi L., Wang J., Wang Z. H. and Shen B. G., *Appl. Phys. Lett.*, **94** (2009) 052105.
[9] Logvenov G., Gozar A. and Bozovic I., *Science*, **326** (2009) 699.
[10] Ohtom O. and Huang H., *Nature*, **427** (2004) 423.

[11] Funahashi R., Matsubara I. and Sodeoka S., *Appl. Phys. Lett.*, **76** (2000) 2385.
[12] Terasaki I., Sasago Y. and Uchinokura K., *Phys. Rev. B*, **56** (1997) R12658.
[13] Masset A. C., Michel C., Maignan A., Hervieu M., Toulemonde O., Studer F., Raveau B. and Hejtmanek J., *Phys. Rev. B*, **62** (2000) 166.
[14] Venkatasubramanian R., Siivola E., Colpitts T. and O'quinn B., *Nature*, **413** (2001) 597.
[15] Habermeier H., *Mater. Today*, **10**, issue No. 10 (2007) 34.
[16] Wang S. F., Venimadhav A., Guo S., Chen K., Li Q., Soukiassian A., Schlom D. G., Katz M. B., Pan X. Q., Ong-Ng W., Vaudin M. D. and Xi X. X., *Appl. Phys. Lett.*, **94** (2009) 02210.
[17] Wang S. F., Zhang Z., He L., Chen M., Yu W. and Fu G., *Appl. Phys. Lett.*, **94** (2009) 162108.
[18] Kawasaki M., Takahashi K., Maeda T., Tsuchiya R., Shinohara M., Ishiyama O., Yonezawa T., Yoshimoto M. and Koinuma H., *Science*, **226** (1994) 1540.
[19] Zhu X., Shi D., Dou S., Sun Y., Li Q., Wang L., Li W., Yeoh W., Zheng R., Chne Z. and Kong C., *Acta Mater.*, **58** (2010) 4281.
[20] Qiao Q., Gulec A., Paulauskas T., Kolesnik S., Dabrowski B., Ozdemir M., Boyraz C., Mazumdar D., Gupta A. and Klie R. F., *J. Phys.: Condens. Matter*, **23** (2011) 305005.
[21] Itoh T. and Terasaki I., *Jpn. J. Appl. Phys., Part 1*, **39** (2000) 6658.
[22] Eng H. W., Limelette P., Prellier W., Simon CH. and Frésard R., *Phys. Rev. B*, **73** (2006) 033403.
[23] Sze S. M., *Physics of Semiconductor Devices*, 2nd edition (Wiley, New York) 1981.
[24] Takeuchi T, Kondo T., Takami T., Takahashi H., Ikuta H., Mizutani U., Funahashi R., Shikano M., Mikami M., Tsuda S., Yokoya T., Shi S. and Muro T., *Phys. Rev. B*, **69** (2004) 125410.
[25] Assmann E., Blaha P., Laskowski R., Held K., Okamoto S. and Sangiovanni G., *Phys. Rev. Lett.*, **110** (2013) 078701.